Fill-Tube-Induced Mass Perturbations on X-Ray-Driven, Ignition-Scale, Inertial-Confinement-Fusion Capsule Shells and the Implications for Ignition Experiments

G. R. Bennett,[1] M. C. Herrmann,[1] M. J. Edwards,[2] B. K. Spears,[2] C. A. Back,[3] E. W. Breden,[1] P. J. Christenson,[1] M. E. Cuneo,[1] K. L. Dannenburg,[3] C. Frederick,[3] K. L. Keller,[1] T. D. Mulville,[1] A. Nikroo,[3] K. Peterson,[1] J. L. Porter,[1] C. O. Russell,[1] D. B. Sinars,[1] I. C. Smith,[1] R. M. Stamm,[1] and R. A. Vesey[1]

[1]*Sandia National Laboratories, Albuquerque, New Mexico 87185-1193, USA*
[2]*Lawrence Livermore National Laboratory, Livermore, California 94550, USA*
[3]*General Atomics, San Diego, California 92186, USA*

(Received 17 March 2007; published 13 November 2007)

On the first inertial-confinement-fusion ignition facility, the target capsule will be DT filled through a long, narrow tube inserted into the shell. μg-scale shell perturbations $\Delta m'$ arising from multiple, 10–50 μm-diameter, hollow SiO_2 tubes on x-ray-driven, ignition-scale, 1-mg capsules have been measured on a subignition device. Simulations compare well with observation, whence it is corroborated that $\Delta m'$ arises from early x-ray shadowing by the tube rather than tube mass coupling to the shell, and inferred that 10–20 μm tubes will negligibly affect fusion yield on a full-ignition facility.

DOI: 10.1103/PhysRevLett.99.205003 PACS numbers: 52.57.Fg, 52.65.−y, 52.70.La

Introduction.—A major goal of inertial-confinement-fusion (ICF) is a demonstration of thermonuclear ignition and gain in the laboratory via the extreme spherical compression and shock-induced heating of cryogenic DT fuel [1]. In the indirect drive ICF approach, an intense Planckian-like x-ray field is applied to a 2 mm diameter, DT-filled low-Z spherical capsule, thus driving a rocketlike, momentum-conserving implosion. This creates a tiny, centrally-located lower-density higher-temperature DT hotspot, surrounded by a higher-density lower-temperature region forming the DT bulk, which in turn is surrounded by the remaining capsule shell material.

The first ignition-capable device, the National Ignition Facility (NIF) [2], to be completed in 2010, will generate drive x rays by the 192 laser-beam irradiation of the interior of a 5-mm diameter, 9-mm length cylindrical high-Z cavity (hohlraum). In terms of the target design, regardless of the eventual capsule material choice—Be, CH, or diamond—NIF ignition experiments will DT fill the capsule *in situ* in the target chamber via a long narrow fill tube that is embedded 5–40 μm into the shell. Here, as with all hotspot ignition concepts, the cryogenic DT fuel mass will be distributed into a thick DT ice layer, coating the shell inner surface and surrounding a central gaseous DT region.

Although the tube, composed of SiO_2 or possibly polyimide, has a small 10–20 μm outside diameter, a few μm wall thickness, and a few ng glue mass at the ablator-tube join, a finite adverse effect upon the implosion uniformity, and thus the gain, must be expected. In this regard, simulations by Edwards *et al.* [3] of the resulting mass perturbation $\Delta m'$ at the shell surface indicate a negligible effect upon the fusion yield. However, experiments to validate this, via backlit x-ray imaging at an existing subignition ICF facility, have not previously been conducted, though unpublished work [4] using target self-emission x-ray imaging has been performed.

Discussion.—In this Letter, $\Delta m'$ perturbations (μg-scale) of shell material induced by hollow, 10–50 μm diam SiO_2 tubes partially embedded in a noncryogenic, NIF-scale 1-mg capsule have been measured, at 1.5–2.5 convergence ratios (Cr). The capsules were indirectly driven on a subignition facility, but the tube evolution details and perturbation masses were similar to those of the NIF low-Cr phase. Significantly, detailed simulations of the experiment using the HYDRA [5] radiation-hydrodynamics code compare closely with the measurements. It is thus corroborated with Edwards *et al.* [3] that $\Delta m'$ arises from an early-time, but short-lived, tube x-ray shadow, rather than the well-studied direct hydrodynamic mass coupling effect of, in this case, tube mass with the shell. The level of experimental validation achieved through this complex phase, perturbation establishment, increases the confidence in HYDRA-predicted perturbations of 10–20 μm tubes on NIF capsules, simulations that indicate a minimal impact upon the fusion yield.

The experiments were performed on Sandia National Laboratories' Z-Accelerator [6] using the well-established 70 eV z-pinch-driven, double-ended-hohlraum (DEH) [7]. To most effectively separate the tube perturbation of interest from possible low-mode shell asymmetries caused by poor drive uniformity, the DEH configuration that was expected to yield the most uniform field was employed: a secondary hohlraum of 19.24 mm diameter and 15.97 mm length. High-spatial-resolution, highly-monochromatic, 6.151 keV curved-Bragg-crystal imaging [8] formed the principal diagnostic. The x-ray backlighting point source was created by Z-Beamlet-Laser ([8] and Refs. therein) irradiation of a Mn target foil, producing 6.151 keV He_α triplet x rays. The imaging spatial resolution is estimated to be 20 ± 5 μm.

 © 2007 The American Physical Society

Implosion images were captured at Cr = 1.55 ± 0.02 and Cr = 2.39 ± 0.02 (capsule initial outer radius/implosion radius of minimum limb-darkened transmission) with the intention that, according to HYDRA simulations (unvalidated then), any tube and glue material would be far from the ablating shell. This would insure that the optical depths forming the image were from known combinations of materials, but the region of interest would not be too small and too low in x-ray transmission to preclude a precise analysis. The experiment used 2.1 mm diameter CH shells as this capsule was the easiest to manufacture and attach fill tubes to. The smoothest such capsules were employed so that the fill tube perturbation could be distinguished from any existing random isolated defects on the shell surface.

The tests discussed here, *A* and *B* (*Z* shots *z*1751 and *z*1755, respectively), used capsules with 2.129 mm diameter and 72.7 μm shell thickness; the inner 34.6 μm was pure CH, and the outer 38.1 μm was CH doped with 0.83% atomic Ge. The doped outer surface served to enhance the contrast of the perturbed material, imaged at 6.151 keV, but without losing finite transmission of the limb-darkened feature, from which the necessary Cr could be accurately measured.

Four holes, approximately 40 microns in depth, were drilled every 90° around a great circle of the capsule. The tubes were inserted, and the oversized shell hole, surrounding the tube, was filled with epoxy, the mass density of which was similar to the CH shell. Efforts were taken to minimize the epoxy fillet sizes, and HYDRA simulations (albeit unvalidated then) indicated little adverse effect for the epoxy volumes used. [HYDRA, a three-dimensional, arbitary Lagrangian Eulerian code, was operated in *rz* geometry (two-dimensions) with the tube on-axis. Implicit Monte Carlo radiation transport was used with 1×10^6 photons.] With three (test *A*) or four tubes (test *B*) per capsule, of different diameter and thickness, the $\Delta m'$ mass perturbation as a function of tube mass per unit length, at a particular Cr, could be conveniently obtained on a single test.

Figure 1 depicts four tubes per capsule (the radiographic axis is out of the paper) and details the capsule/tube interface. Test *A* consisted of three thin wall SiO_2 tubes, 1, 2, & 4 of respective 11.53, 26.03, & 43.76 μm outer diameters, and 3.54, 7.68, & 11.85 μm wall thicknesses. Test *B* consisted of four tubes, 1, 2, 3, & 4 of respective 14.50, 17.88, 33.56, & 45.62 μm diameters, and 4.73, 4.73, 9.47, & 10.93 μm wall thicknesses. The test *A* and test *B* targets were therefore rather similar in terms of the tubes sizes, but they were probed at different times to obtain data at two values of Cr. A static x-ray image of target A1, the smallest tube studied, is shown in Fig. 2 (the 6.151 keV curved-Bragg-crystal imaging system was not used to obtain this image).

Qualitative comparison: simulation vs experiment.—Figure 3 shows the captured x-ray image of test A4 (Cr = 1.55)—a tube *different* to the one in Fig. 2—over

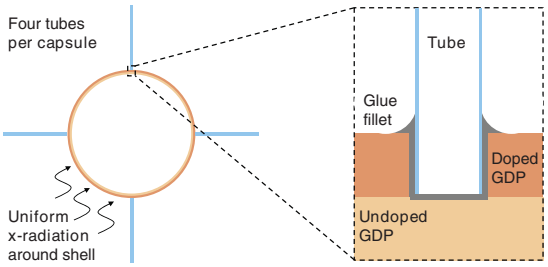

FIG. 1 (color). Schematic illustrating multiple, independent tubes on a capsule (the radiographic axis is out of the paper) and the tube-capsule interface details.

a 200×200 μm^2 view. Transmission contours at 6.151 keV (white and black lines) range over $T_{6.151}$ = 0.4–0.9, in 0.1 increments. The grayscale covers T = 0.35–0.95 (dark-, medium-, light-blue: low-, medium-, high-transmission). HYDRA-simulated contours (red lines) of the same $T_{6.151}$ = 0.4–0.9 span, in 0.1 steps, are overlaid. Left to right, the eight simulated lines represent T = 0.5, 0.4, 0.4, 0.5, 0.6, 0.7, 0.8, and 0.9. The noisy experimental contours at $x \leq -50$ μm (white lines) are of no relevance to the perturbation mass measurement.

The $x \geq -50$ μm region of the image smoothly increases in transmission, left to right. The large blank area left of $x \geq -50$ μm is $T < 0.35$. The perturbation consists of C/H/Ge plasma and any tube plasma (Si and O) is at large positive x, outside of the region shown. Visually, the simulation, which includes spatial resolution and motional blur, compares well to experiment in terms of qualitative width and length of the perturbation, as well as the spacing between contours along the $y = 0$ line.

The test *A* (test *B*) simulated implosion was driven by the measured capsule drive, and the HYDRA information was captured when the (defined) convergence ratio was 1.55 (2.39). Most likely due to uncertainties in the measured drive, the times of Cr = 1.55 and 2.39 in the simulations were slightly different to experiment. By adjusting

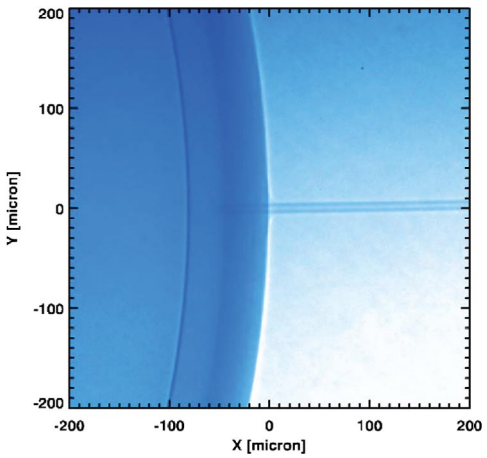

FIG. 2 (color). Static x-ray image of target A1, the smallest tube (11.53 μm diameter) studied.

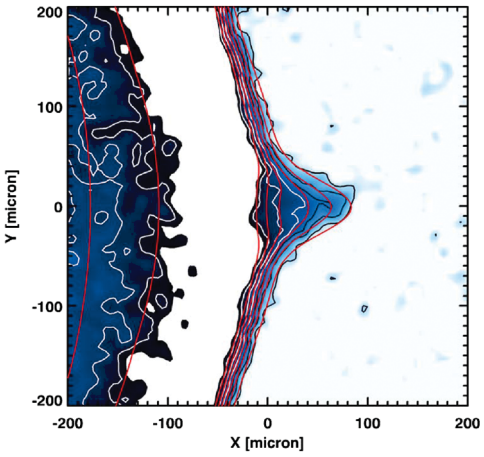

FIG. 3 (color). Measured 6.151-keV x-ray transmission contours (white and black lines) of implosion A (Cr = 1.55), showing the perturbation initiated by the x-ray drive shadow cast from tube A4 (tube A1 is shown in Fig. 2). For $x \geq -50$ μm, 6.151 keV transmission contours range 0.4 (left) to 0.9 (right) in 0.1 increments. HYDRA-simulated contours (red lines) also cover $T = 0.4$–0.9 in 0.1 increments. The grayscale ranges over $T = 0.35$–0.95, and the $T < 0.35$ region appears as white.

the drive prescription in HYDRA, however, to attain the measured Cr at the experimentally measured image capture time, a negligible change in the perturbation was apparent.

Given the qualitative (e.g., Fig. 3) and quantitative (to be discussed shortly) level with which HYDRA simulations compare to experiment, it is evident that this tool may be used to obtain a physical insight in to the effects leading to the perturbation shown in Fig. 3 (test A4 at Cr = 1.55). For instance, at times well before the peak of the 70 eV capsule drive, the expanding C/H/Ge ablator plasma and the Si/O plasma of the exploding tube move towards each other, but in such a way that the Planckian flux is shadowed over an increasing area by the expanding tube material.

Later, the expanding tube material nearest the capsule shell is recompressed by the ablating C/H/Ge plasma, but the ablation front continues to move radially inwards; thus, the shadowing effect reduces. Later still, the Si/O plasma expands again—eventually to a density that is transparent to the x-ray drive radiation. Once the shadowing effect is negligible, Cr > 1.5, the capsule implodes in a conventional fashion, and the perturbation grows in amplitude via the Rayleigh-Taylor (RT) instability [[9] and Refs. therein], an effect that has been well studied experimentally and computationally. As the implosion decelerates, the larger momentum of the perturbation carries it through the shell and the feature inverts.

The connection to ignition experiments.—The NIF conditions during Cr = 1 to Cr = 1.5–2.5 are different; a heavier 4 mg cryogenic capsule is driven by 80–90 eV radiation, and larger ablated mass fractions [10] result. However, these experiments are still relevant to NIF for three reasons. (1) The same phenomena on Z and NIF are predicted by HYDRA. For instance, simulations of the NIF case predict the same overall development as outlined here: tube expansion, compression, and then minimal shadowing, with the perturbation created by radiation shadowing rather than hydrodynamic coupling of tube mass to the capsule shell. (It is noted that calculations of direct tube/capsule hydrodynamic coupling, which is well studied in ICF, are unable to explain the Z data.) (2) Similar tubes show similar mass perturbations on Z and NIF at similar convergence ratios. And (3), after the x-ray shadow vanishes, the perturbation grows via the RT instability. To this end, the Z studies have a good level of surrogacy to NIF ignition experiments.

Quantitative comparison: simulation vs experiment.—A study of the 6.151 keV x-ray opacity, $k_{6.151}(x, y, z)$ [11], in the test A and B HYDRA simulations indicate a minimal variation of the opacity around the perturbation and inside the shell, that is, minimal x, y, z dependence. In this special case, the mass M viewed within a rectangular area of the x, y plane of an x-ray image—Fig. 3 for example—can be measured using $T_{6.151}(x, y)$ as follows:

$$M \cong \frac{-1}{\langle k_{6.151} \rangle} \iint Ln[T(x, y)]dxdy, \tag{1}$$

where the exact $T(x, y) = \exp[-\int k_{6.151}(x, y, z) \times \rho(x, y, z)dz]$ equation is approximated to $T(x, y) \cong \exp[-\langle k_{6.151} \rangle \int \rho(x, y, z)dz]$, and where $\langle k_{6.151} \rangle = \iiint k_{6.151}(x, y, z)dxdydz / \iiint dxdydz$. The z integration limits are through the entire range of the simulation, whereas the x, y limits are those defined by the chosen region of interest, a square or rectangle around the perturbation. For the simulations of interest, $\langle k_{6.151} \rangle = 23$ cm^2/g.

By applying Eq. (1) to the radiograph shown in Fig. 3 (tube A4), and to the radiographs of the other tubes (A1, A2, B1, B2, B3, and B4), measurements of M are obtained. However, they are sensitive to the uncertainty in transmission at low T. To counter this effect, the integration is performed over $0.50 \leq T \leq 0.88$ for test A and $0.35 \leq T \leq 0.88$ for test B, so that low (and high) T contributions are excluded from the integration, but the medium T area of the perturbation remains. M is now a "reduced" mass, the mass within $0.50 \leq T \leq 0.88$ for test A and $0.35 \leq T \leq 0.88$ for test B; it is renamed M'. $\Delta m'$, the reduced mass of the perturbation, is M' with the reduced mass of a similarly sized, unperturbed part of the shell subtracted.

To determine $\Delta m'$, integrations are performed over unperturbed regions above & below the perturbation—over $y = -200$, -150 μm (lower) & $y = 150$, 200 μm (upper)—and the perturbed region, over $y = -100$, 100 μm (in all cases, $x = -100$, 200 μm). By subtracting twice the top integration and twice the lower one from the latter, $\Delta m'$, within the prescribed range of T, is obtained. In addition to circumventing significant mass inaccuracies at low T, $\Delta m'$ has the added advantage that it is insensitive to sufficiently small tilts of the tube (around the y-axis) from perpendicular to the radiographic axis. For comparison

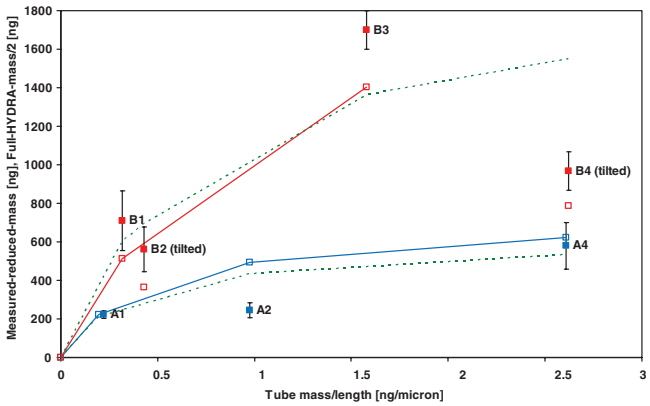

FIG. 4 (color). Reduced mass $\Delta m'$ [ng] as a function of tube mass per unit length [ng/μm] for Cr = 1.55 (experiment, solid blue squares; HYDRA, empty blue squares and blue line) and Cr = 2.39 (experiment, solid red squares; HYDRA, empty red squares and red line). Full HYDRA-predicted masses, but divided by 2 for trend comparisons only, are indicated by the lower (upper) dashed green line for Cr = 1.55 (Cr = 2.39).

purposes, the same quantity is easily extracted from HYDRA-simulated radiographs.

Figure 4 plots $\Delta m'$ [ng] as a function of tube mass/length [ng/μm] for Cr = 1.55 (experiment, solid blue squares; HYDRA, empty blue squares and blue line) and Cr = 2.39 (experiment, solid red squares; HYDRA, empty red squares and red line). For completeness, the full $0.00 \leq T \leq 1.00$ perturbation mass from simulation, but divided by 2 for trend comparison only, is indicated by the lower (upper) dashed green line for Cr = 1.55 (Cr = 2.39).

The simulations compare well with the data, for all but test A2. (At this writing, the anomalous result is not understood.) The *in situ* preshot radiograph of test *B* indicates that tubes B2 and B4 are tilted 15° with respect to the normal of the radiographic axis, an angle too large for a determination of the small-angle-independent $\Delta m'$ metric. Applying the same tilt to the respective HYDRA-simulated radiographs yielded $\Delta m'$ values close to those measured, as shown in Fig. 4, the empty red squares below the solid red squares labeled B2 (tilted) and B4 (tilted). Notably, all of the measured masses are μg-scale, 0.1% of the 1.06 mg capsule mass.

Edwards *et al.* [3] predict that the mass within the 1°–4° polar angle range (0° corresponding to the $y = 0$ line of Fig. 3) of a perturbation is linear with tube diameter, for a constant ratio of outer diameter to inner diameter. That is, the perturbation mass is proportional to the square root of the tube mass per unit length. In the *Z* experiments, it is observed that $\Delta m'$, the (reduced) mass (including 0°–1° angles) has a similar square root dependence on the tube mass per unit length.

With experimental validation through the transient x-ray shadow phase, it is now reasonable to address with confidence the conclusions of full history HYDRA simulations on NIF, calculations that transition to RT growth of $\Delta m'$. In particular, the pertinent conclusions of Edwards *et al.* [3] are examined. Most importantly, 10–20 μm SiO_2 tubes—similar to some of those studied here—are predicted to only slightly affect the fusion yield compared with that of the ideal one-dimensional case.

In Conclusion.—Capsules for thermonuclear ignition and gain experiments on NIF, beginning 2010, will be DT filled via a long, narrow tube placed part way into the shell. Here, the mass perturbation (shell material and μg-scale) on the exterior of a noncryogenic, NIF-scale, 1.06 mg capsule, arising from hollow 10–50 μm diameter SiO_2 tubes, have been measured at Cr = 1.5–2.5 on a subignition facility. The tube evolution details and the perturbation masses are similar to those of the NIF low-Cr phase. The perturbation is fully established at early times, Cr < 1.5, and thereon grows via the RT instability. HYDRA compares closely with experiment; thus, a level of validation has been attained for this important ICF computational design tool, a tool that suggests a negligible effect on NIF's fusion yield for the smallest tubes investigated here.

The authors wish to thank S. W. Haan, M. M. Marinak, and H. F. Robey of Lawrence Livermore National Laboratory (LLNL) for helpful discussions, and LLNL for access to HYDRA and the associated computer time. Sandia is a multiprogram laboratory operated by Sandia Corporation, a Lockheed Martin Company, for the National Nuclear Security Administration under No. DE-AC04-94AL85000.

[1] J. D. Lindl *et al.*, Phys. Plasmas **11**, 339 (2004).
[2] G. H. Miller *et al.*, Nucl. Fusion **44**, S228 (2004).
[3] M. J. Edwards *et al.*, Phys. Plasmas **12**, 056318 (2005).
[4] N. Izumi *et al.*, http://meetings.aps.org/Meeting/DPP06/Event/54918, http://meetings.aps.org/Meeting/DPP05/Event/34958.
[5] M. M. Marinak *et al.*, Phys. Plasmas **8**, 2275 (2001).
[6] M. K. Matzen *et al.*, Phys. Plasmas **12**, 055503 (2005).
[7] M. E. Cuneo *et al.*, Phys. Rev. Lett. **88**, 215004 (2002); R. A. Vesey *et al.*, *ibid.* **90**, 035005 (2003); G. R. Bennett *et al.*, *ibid.* **89**, 245002 (2002); R. A. Vesey *et al.*, Phys. Plasmas **10**, 1854 (2003); G. R. Bennett *et al.*, *ibid.* **10**, 3717 (2003); M. E. Cuneo *et al.*, Plasma Phys. Controlled Fusion **48**, R1 (2006); R. A. Vesey *et al.*, Phys. Plasmas **14**, 056302 (2007).
[8] D. B. Sinars *et al.*, Rev. Sci. Instrum. **75**, 3672 (2004); G. R. Bennett *et al.*, Rev. Sci. Instrum. **77**, 10E322 (2006).
[9] S. Atzeni and J. Meyer-Ter-Vehn, *The Physics of Inertial Fusion* (Clarendon Press, Oxford, 2004), p. 237–299.
[10] For Cr = 1.5–2.5, the ablated mass fraction on *Z* is 30% (capsule is coasting for Cr > 1.5), but 65% and 80%, respectively, on NIF.
[11] Here, the *z*-axis is of the Cartesian coordinate system, not the cylindrical axis of the two-dimensional *rz* HYDRA simulations.